Relativistic effects on polarization transfer observables for quasielastic proton-nucleus scattering

G. C. Hillhouse* and P. R. De Kock
University of Stellenbosch, Stellenbosch 7600, South Africa
and National Accelerator Centre, Faure 7131, South Africa
(Received 25 June 1993)

Within the relativistic plane-wave impulse approximation, the sensitivity of complete sets of quasielastic proton-nucleus spin observables is investigated with respect to relativistic effects, the importance of exchange contributions to the NN amplitudes, the form of the πN vertex, and spin-orbit distortions. Calculations are performed at laboratory energies ranging from 135 to 500 MeV and for target nuclei ranging from ^{12}C to ^{208}Pb at a fairly large fixed momentum transfer of 1.97 fm^{-1}. Of all the spin observables, only A_y exhibits a clear relativistic effect at the highest energy, as has been previously found. However, at the lower energies (200 MeV and below) the relativistic effect shifts to two other polarization transfer observables, mainly $D_{s's}$ and to a lesser extent $D_{l's}$. In addition, it is found that $D_{n'n}$ is extremely sensitive to the pseudoscalar versus pseudovector ambiguity of the πN vertex, whereas $D_{s'l}$ and $D_{l'l}$ are sensitive to exchange contributions to the NN amplitudes. Compared to the latter, the effects of spin-orbit distortion are not insignificantly small and had to be corrected for. This investigation stresses the urgent need for measurements of the quasielastic spin observables at these low energies.

PACS number(s): 24.10.Jv, 24.70.+s, 25.40.−h

I. INTRODUCTION

The real advantage of Dirac relativistic mechanics lies in its natural description of a particle's spin as well as the accommodation of particle-antiparticle excitations in strong fields. Hence, the interaction of a medium energy nucleon with a nucleus is in the relativistic domain and the Dirac equation will, via the spin dependence of the nuclear force, play a vital role in the description of its polarization observables.

In recent years several elastic and inelastic proton-nucleus spin observables have been analyzed using relativistic models based on the Dirac equation. For a recent review see Ref. [1]. Despite the success of the relativistic predictions of scattering observables [2–5], present state-of-the-art Schrödinger-based, nonrelativistic calculations describe the data just as well [6], if not better.

The clearest relativistic effect to date is that of the analyzing power A_y for inclusive $(\vec{p},\vec{p}')$ scattering from ^{40}Ca and ^{208}Pb at 500 MeV [7]. In the case of both nuclei, the relativistic prediction has been spot on, while all nonrelativistic methods up to the present overestimate the experimental values by $\sim 40\%$ and thus fail completely. However, most of the other five independent spin transfer observables allowed by parity and time-reversal invariance, $D_{n'n}, D_{s's}, D_{l'l}, D_{s'l}$, and $D_{l's}$, seem to favor the nonrelativistic calculation. (In each $D_{i'j}$ the primed and unprimed subscripts refer to outgoing and incoming spin directions, respectively [7].)

This inconsistency requires some deeper investigation. Therefore, one of the aims of this paper is to calculate complete sets of spin observables in more improved ways. The question also arises as to how sensitive the observables are to relativistic effects at energies appreciably lower than 500 MeV. The reason for this is that, as the energy is lowered, the magnitudes of the (real part of) the Dirac scalar and vector optical potentials, which additively contribute to spin observables, both increase, and this may enhance the relativistic effect on spin observables other than A_y. Therefore this investigation also entails in total the sensitivity to relativity of all the spin observables for quasielastic proton scattering from various nuclei at five fixed intermediate energies ranging from (as low as) 135 to 500 MeV.

Inclusive quasielastic scattering of protons can be viewed as a fairly elastic collision with a single target nucleon near the nuclear surface [8]. It manifests itself in the inclusive continuum energy spectrum as a broad peak, the maximum of which corresponds to an energy transfer of $\omega \approx \mathbf{q}^2/2m$ ($\mathbf{q}$ being the transferred momentum) and the width of which is due to the momentum distribution of the target nucleons [9]. Quasielastic scattering at the peak thus approximately simulates free nucleon-nucleon (NN) scattering and is therefore an ideal testing ground for the medium-modified NN interaction. For the present full proton energy range of 135 to 500 MeV, ω ranges from 0 to 100 MeV and the associated $|\mathbf{q}|$ from 1 to 2 fm^{-1}. These transfers are sufficiently large to adequately separate the quasielastic peak from proton peaks resulting from low-lying discrete states and resonances.

Essentially the formalism and analysis employ the relativistic plane wave impulse approximation (RPWIA) model (Sec. II A), developed by Horowitz and Iqbal [10] and Horowitz and Murdock [7].

We now mention the improvements of the present cal-

*Present address: University of the Western Cape, Bellville 7530, South Africa.

culations. Firstly, ambiguities in the form of the NN interaction are studied by employing a meson exchange model for the NN interaction (presently the Horowitz-Love-Franey model), rather than the Wolfenstein-type parametrization of the Arndt phase shifts. Secondly, the relativistic effect is contained in an effective nucleon mass of both projectile and target nucleons interacting in the surrounding nuclear medium. Preliminary calculations indicate the sensitivity of the spin observables with respect to these effective mass values. Our present refinement in calculating effective mass values is based on a self-consistent (Dirac-) Hartree calculation of effective masses.

We demonstrate for the first time the enhanced sensitivity of complete sets of spin observables to certain aspects of the RPWIA at energies as low as 135 MeV.

For a proper handling of the NN interaction in quasielastic nucleon scattering, medium effects of the surrounding nucleus have to be corrected for. They are treated here as distortions of the Dirac free particle wave function by the nuclear potential and, as distortions are generally larger on low energy particle waves, they deserve some special attention in the present analysis. After dealing with the RPWIA formalism in Sec. II A, Sec. II B presents the calculation of the effective nucleon masses which contain the distortion by the central part of the optical potential. Section II C presents the distortion by the spin-orbit potential which effectively rotates both initial and final state spinors, and in this way directly affects the spin observables. The Horowitz-Love-Franey NN interaction with its exchange [11] is discussed in Sec. II D and, finally, all the theoretical aspects are tested in the calculation of the spin observables in Sec. III. Section IV summarizes our final conclusions.

II. RELATIVISTIC PLANE-WAVE IMPULSE APPROXIMATION (RPWIA)

A. Formalism

The RPWIA is described in Ref. [7]. This model allows one to investigate medium modifications of the NN interaction through the accompanying enhancement of the lower components of projectile and target nucleon Dirac wave functions which result from the strong and opposing scalar and vector potentials. We denote the laboratory momenta and spin of the incident nucleon by $\{\mathbf{k}_1, s_1\}$ before, and $\{\mathbf{k}'_1, s'_1\}$ after its scattering, and similarly for the target nucleon by $\{\mathbf{p}_2, s_2\}$ and $\{\mathbf{p}'_2, s'_2\}$ before and after the scattering respectively. Then, for example, the four-component Dirac spinor for the projectile is (in natural units, $\hbar = c = 1$)

$$U_1^*(\mathbf{k}_1, s_1) = \left(\frac{E_1^* + m_1^*}{2m_1^*}\right)^{1/2} \begin{pmatrix} 1 \\ \frac{\sigma \cdot \mathbf{k}_1}{E_1^* + m_1^*} \end{pmatrix} \chi_1 \,, \tag{1}$$

where χ_1 is a two-component Pauli spinor of projection s_1 and

$$E_1^* = (\mathbf{k}_1^2 + m_1^{*2})^{1/2} \,, \tag{2}$$

with similar expressions for the other nucleons involved in the collision. m^* is the effective nucleon mass (Sec. II B).

Using the conventions of Bjorken and Drell [12], the invariant matrix element for quasielastic proton-nucleus scattering is given by

$$\mathcal{M} = \overline{U}_1^*(\mathbf{k}'_1, s'_1) U_1^*(\mathbf{k}_1, s_1) \mathcal{T}(\mathbf{q}, E) \overline{U}_2^*(\mathbf{p}'_2, s'_2) U_2^*(\mathbf{p}_2, s_2) \tag{3}$$

with E the incident laboratory energy. $\mathcal{T}$ is the form of the invariant NN scattering operator used in the original relativistic impulse approximation (RIA) [2] and is expressed as

$$\mathcal{T}(\mathbf{q}, E) = \sum_{i=1}^{5} T_i(\mathbf{q}, E) \lambda_i^{(1)} \cdot \lambda_i^{(2)} \,, \tag{4}$$

where the superscripts (1) and (2) refer to the projectile and target nucleons, respectively, the i's stand for the five Dirac matrix types listed in Table I, and the dot product implies that the Lorentz indices are contracted.

The amplitudes $T_i(\mathbf{q}, E)$ can be parametrized in terms of an appropriate model (see Sec. II D) for the NN interaction or can be related to the experimental NN amplitudes. They are normalized in the usual way [2, 7, 10, 11] by equating the matrix elements of Eq. (3) for free Dirac spinors U (spinors with $m^* = m$, the free nucleon mass) to the Wolfenstein amplitudes.

Once $\mathcal{M}$ is fully known, the spin observables can be calculated from the usual expressions as in Ref. [7]. At the high excitation energies of interest, shell effects are unimportant and hence a Fermi gas should be an appropriate model for the target nucleus [9]. Consequently, all the spin observables need to be averaged over the Fermi distribution of the momenta of the target nucleons which range from a certain minimum value up to the Fermi momentum (see Sec. II B). For each value of target nucleon momentum, the NN amplitudes have to be evaluated at an effective laboratory kinetic energy T_L^{eff} and an effective center of mass scattering angle. For inclusive quasielastic $(\vec{p}, \vec{p}')$ scattering, the spin observables need of course to be calculated as appropriate averages of those for pp and pn scattering.

Note that by a "relativistic" or "m^* effect" we refer to the value of a spin observable calculated with an effective mass in Eq. (3) relative to the corresponding calculation using the free nucleon mass m.

TABLE I. Dirac matrix types used in the text.

$$\mathcal{T}(\mathbf{q}, E) = \sum_{L=1}^{5} T_L(\mathbf{q}, E) \lambda_L^{(1)} \cdot \lambda_L^{(2)}$$

L	λ_L
S (scalar)	1
V (vector)	γ_μ
P (pseudoscalar)	γ_5
A (axial vector)	$\gamma_5\gamma_\mu$
T (tensor)	$\sigma_{\mu\nu}$

B. Effective mass

The concept of an effective mass for a Dirac particle in the field of a medium has been introduced in the mean field theory (MFT) of Serot and Walecka [13]. In this MFT, the Dirac fields are replaced by their mean values:

$$S(\mathbf{r}) \to \langle S \rangle \quad \text{and} \quad V(\mathbf{r}) \to \langle V \rangle \ ,$$

which lead to a truly free particle Dirac equation with, however, an effective mass:

$$m^* = m + \langle S \rangle \ . \tag{5}$$

In the present analysis of quasielastic scattering, the effective masses of both the projectile and target nucleon (m_1^* and m_2^*, respectively) are calculated. $S(\mathbf{r})$ is averaged over the whole nucleus by weighting it with $T(b)$, the transmission probability through the nucleus at impact parameter b, and with the nuclear density $\rho(\mathbf{r})$ of the specific nucleus, analogous to the method of Horowitz and Iqbal [10, 14]. The latter used in their analysis, however, the functions $S(\mathbf{r})$ and $\rho(\mathbf{r})$ of Kobos and Cooper [15] to calculate only m_1^* for the incoming protons; both functions being restricted to a Woods-Saxon form. For m_2^* of the target nucleons they employed simply a mean scalar field for nuclear matter in Eq. (5), which relies on the reasonable assumption that $S(\mathbf{r}) = \alpha\rho(\mathbf{r})$, but with constant α applying to infinite nuclear matter.

Our aim was also to employ the most recent and refined functions for the Dirac optical potentials and nuclear densities. We therefore concentrated on those resulting from an investigation of Horowitz, Murdock, and Serot [16] who analyzed the mutual interaction of nucleons in a nucleus by relativistic fields describing the exchange of mesons as in the Walecka model [13] and performed selfconsistent (Dirac-) Hartree calculations to obtain the fields. [They limited it to spherical symmetrical closed shell nuclei, which restricted the meson fields to the zero component of the vector field $V^0(\mathbf{r})$ and the scalar field $\phi(\mathbf{r})$.] The resulting field equation for the baryons becomes a Dirac equation with $-g_s\phi(\mathbf{r})$ as the scalar potential, adding to the baryon mass, with g_s being the scalar meson coupling constant. In the present case we consider $-g_s\phi(\mathbf{r})$ to be the scalar potential for the struck nucleon and therefore, in the mean field approximation, its effective mass becomes:

$$m_2^* = m - g_s\langle\phi\rangle \ . \tag{6}$$

We presently employ the computer code TIMORA of Horowitz *et al.* [17] to calculate, in the self-consistent (Dirac-) Hartree formulation, the potential $\phi(\mathbf{r})$ for a specific nucleus, as well as the scalar and baryon density functions $\rho_s(\mathbf{r})$ and $\rho_B(\mathbf{r})$. After averaging $\phi(\mathbf{r})$ over the nucleus as described above, we could calculate m_2^* from Eq. (6).

The calculation of m_1^* from Eq. (5) requires a scalar optical potential $S(\mathbf{r})$ for the projectile nucleon. This potential has been obtained by folding, according to the RIA formalism, the components of a NN interaction t matrix with the scalar and baryon densities $\rho_s(\mathbf{r})$ and $\rho_B(\mathbf{r})$ of the specific nucleus. In this t matrix we apply for consistency the same Horowitz-Love-Franey NN interaction which is to be used in the transfer matrix [$\mathcal{T}$ of Eqs. (3) and (4)] for the spin observables and include pseudovector coupling, which formerly [2] yielded by far the best agreement with phenomenological Dirac optical potentials. We used the code FOLDER of Ref. [17] for the folding procedure to obtain the optical potentials, the scalar potential of which has been averaged to obtain the appropriate m_1^* values.

Table II lists the effective nucleon mass values (as $M^* = m^*/m$, with m being the free nucleon mass) presently calculated for the $(\vec{p}, \vec{p}')$ scattering from the nuclei ^{12}C, ^{16}O, ^{40}Ca, ^{54}Fe, and ^{208}Pb, each at proton laboratory energies of 135, 200, 300, 400, and 500 MeV. These are listed as $M_{1\mathrm{SC}}^*$ and $M_{2\mathrm{SC}}^*$ for the projectile and target nucleons respectively, where the subscript SC denotes the self consistent optical potentials. The last three columns list, respectively, $\langle b \rangle$, the mean impact parameter, $k_F = (\frac{3}{2}\pi^2\langle\rho_B\rangle)^{\frac{1}{3}}$, the Fermi momentum, and A_{eff}, the effective number of struck nucleons, the latter being of course in the nuclear surface. For comparison, the corresponding effective masses have also been calculated with a more recent phenomenological optical potential, a global Dirac optical potential formula, developed by Cooper [5] from fits to empirical data. These M^* values, subscripted by CP (Cooper potentials), are also included in Table II. The reasonable agreement between the sets of M_{SC}^* and M_{CP}^* values is expected since the corresponding optical potentials are fairly similar. Table II also contains the formerly calculated M^* values, mentioned above and reported in Ref. [7], and are subscripted by HM (Horowitz and Murdock).

We now analyze the general trends exhibited by both the SC and CP sets of effective mass values. Firstly, for scattering in a specific nucleus, the effective masses of both projectile and target nucleons increase with projectile laboratory energy T_{lab}, the increase of that of the projectile being larger. This can be explained as follows: As T_{lab} increases, more channels generally open for projectile absorption inside the nucleus, which manifests itself as an increase of the imaginary part of the optical potential. This decreases the projectile's transmission $T(\mathbf{b})$ through the inner nucleus and shifts the region of proton scattering more to the nuclear surface, where the magnitudes of all nuclear potentials start to decline substantially. Therefore, as T_{lab} increases, both $\langle\phi\rangle$ and the magnitude of the real part of $\langle S \rangle$ decrease and, with S being negative, this leads to an increase of both m_1^* and m_2^*, according to Eqs. (5) and (6), respectively. In addition, it is known that, as T_{lab} increases, the magnitude of the real part of the Dirac optical potential function $S(\mathbf{r})$ decreases at all $\mathbf{r}$ [2]. This leads to a further reduction in $\langle S \rangle$ and thus a further increase in m_1^*, as Table II shows.

Secondly, m_1^* and m_2^* do not vary significantly with the mass number of the scattering nucleus. Note, however, that the effective number of (surface) nucleons acting as scatterers, A_{eff} (Table II), does not increase as much with nuclear size. This means that for heavier scattering nuclei, the scattering becomes more surface peaked, and there is more of a free nucleon interaction in which the remaining (heavy) nucleus plays a minor role. This is

also reflected by the m_1^* values very near to the free mass value, as was found for ^{208}Pb. On the other hand, the lightest nucleus, ^{12}C, is more penetrated by the incident beam and, on average, a third of all the nucleons partake in the scattering. Thus, using quasielastic scattering, medium effects are, contrary to initial intuition, better studied with scattering by light nuclei. This is also reflected by the relatively low effective mass values for ^{12}C.

The real effect of these M^* values will be discussed in Sec. III, where they have been employed in calculating spin observables.

C. Spin-orbit distortion

In calculating the nucleon transmission probability $T(b)$ in Sec. II B, only the central part of the (effective Schrödinger) optical potential has been employed. The inclusion of a spin-orbit part leads only to an additional space rotation of both initial and final state vectors. Averaging this effect over the whole nucleus leads to a net rotation along an axis perpendicular to the scattering plane only [10]. This rotation directly affects the eventual spin observables.

Figure 1 presents graphically the amount of spin-orbit distortion on all six the spin observables $A_y, D_{n'n}, D_{s's}, D_{l'l}, D_{s'l}$, and $D_{l's}$ as a function of the five chosen laboratory energies; these have all been calculated at the centroid of the quasielastic peak for proton scattering by ^{40}Ca ($|\mathbf{q}|= 1.97$ fm^{-1}). The graphs show that the spin-orbit distortion is indeed not a negligible factor; although being fairly constant with laboratory energy $T_{\rm lab}$, its relative values increase as $T_{\rm lab}$ decreases. At low energies ($T_{\rm lab} \leq 200$ MeV) the spin-orbit effect becomes comparable with the presently investigated phenomenological effects (relativity and the form of the πN vertex), therefore all spin observables presented in Sec. III have been corrected for spin-orbit distortion.

Figure 2 presents the spin-orbit distortion of the six spin observables as a function of nuclear mass. These are calculated again at the centroid of the quasielastic peak, but at a fixed laboratory energy $T_{\rm lab} = 200$ MeV. Its general increase with nuclear size agrees with the natural expectation.

The very small distortion effect on the $D_{n'n}$ values deserves some physical explanation: If the spin rotation angle R, with its axis perpendicular to the scattering plane, would be completely real, this rotation would have no effect on $D_{n'n}$, which relates polarization components that are also perpendicular to the scattering plane. However, due to the small absorptive part of the optical potential, R has a small imaginary part (typically $R = \pm 0.15 \pm 0.05i$

TABLE II. Average effective masses, impact parameters, Fermi momenta, and effective number of struck nucleons for various nuclei and laboratory kinetic energies.

Target nucleus	$T_{\rm lab}$ (MeV)	$M^*_{\rm 1SC}$	$M^*_{\rm 2SC}$	$M^*_{\rm 1CP}$	$M^*_{\rm 2CP}$	$M^*_{\rm 1HM}$	$M^*_{\rm 2HM}$	$\langle b \rangle$ (fm)	k_F (fm^{-1})	$A_{\rm eff}$
^{12}C	135	0.762	0.762	0.836	0.754			2.109	1.059	4.210
^{12}C	200	0.795	0.768	0.853	0.775	0.850	0.840	2.136	1.050	4.443
^{12}C	300	0.832	0.772	0.868	0.792			2.162	1.042	4.482
^{12}C	400	0.862	0.786	0.883	0.807	0.860	0.840	2.243	1.020	4.156
^{12}C	500	0.890	0.799	0.892	0.814	0.910	0.870	2.331	0.996	3.636
^{16}O	135	0.847	0.779	0.828	0.765			2.409	1.029	4.875
^{16}O	200	0.839	0.781	0.846	0.782			2.421	1.026	5.311
^{16}O	300	0.855	0.786	0.862	0.798			2.458	1.017	5.302
^{16}O	400	0.870	0.796	0.871	0.809			2.529	1.000	5.016
^{16}O	500	0.893	0.809	0.885	0.815			2.631	0.976	4.330
^{40}Ca	135	0.836	0.778	0.810	0.749			3.434	1.024	6.736
^{40}Ca	200	0.832	0.784	0.832	0.771	0.82	0.81	3.484	1.014	7.277
^{40}Ca	300	0.847	0.787	0.851	0.789			3.510	1.008	7.496
^{40}Ca	400	0.864	0.798	0.865	0.799	0.83	0.80	3.599	0.989	7.133
^{40}Ca	500	0.892	0.817	0.879	0.810	0.90	0.85	3.759	0.955	5.973
^{54}Fe	135	0.819	0.757	0.796	0.722			3.753	1.055	6.494
^{54}Fe	200	0.817	0.766	0.819	0.748			3.822	1.041	7.066
^{54}Fe	300	0.833	0.770	0.840	0.769	0.86	0.85	3.850	1.034	7.378
^{54}Fe	400	0.853	0.783	0.855	0.781			3.948	1.012	7.044
^{54}Fe	500	0.885	0.805	0.874	0.794			4.123	0.974	5.811
^{208}Pb	135	0.828	0.835	0.807	0.767			6.929	0.986	7.670
^{208}Pb	200	0.845	0.831	0.842	0.801	0.82	0.82	6.880	0.922	9.572
^{208}Pb	300	0.860	0.825	0.866	0.822			6.808	0.934	11.140
^{208}Pb	400	0.885	0.836	0.885	0.839	0.86	0.83	6.913	0.911	11.033
^{208}Pb	500	0.916	0.857	0.896	0.850	0.88	0.85	7.114	0.868	9.146

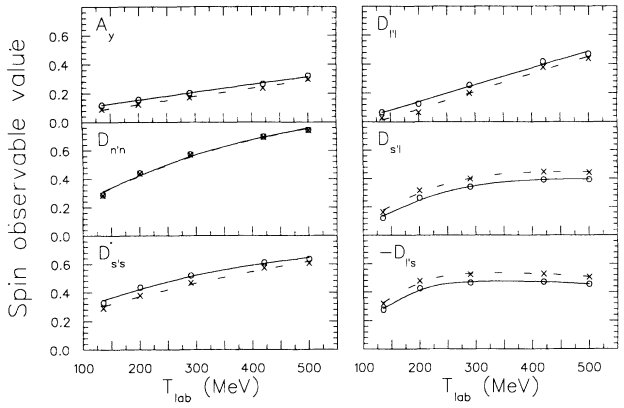

FIG. 1. The spin-orbit distortion of the polarization transfer observables $D_{i'j}$ is illustrated as function of the laboratory energy $T_{\rm lab}$. For each observable the open circles and crosses display the respective undistorted and spin-orbit distorted values at specific laboratory energies. The solid and dashed lines serve merely to guide the eye.

rad), which leads to a generally nonunitary rotation operation on the state vectors, in which case $D_{n'n}$ might be slightly affected. The explicit expression for the spin-orbit distortion of $D_{n'n}$ (Eqs. (40) and (41) in Ref. [10]) also displays this dependence on only the imaginary part of R.

This insensitivity of $D_{n'n}$ to spin-orbit distortion enhances, however, its value as a probe for important NN interaction effects (see Sec. III).

D. The Horowitz-Love-Franey (HLF) t matrix

The nucleon-nucleon (NN) t matrix employed in this work is based on a relativistic Love-Franey formalism that is described in detail in Refs. [11, 17] and will be referred to as the HLF (Horowitz-Love-Franey) model. We use the HLF model to investigate the importance of exchange and also to study the influence of different

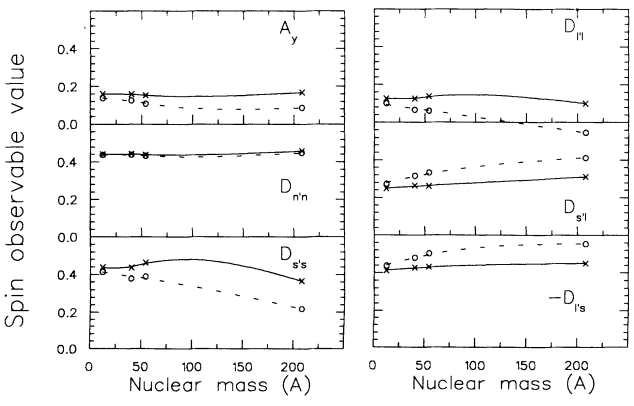

FIG. 2. The same as for Fig. 1, but here the spin-orbit distortion of the polarization transfer observables $D_{i'j}$ is illustrated as function of the mass number of the scatterer nucleus and at a fixed laboratory energy $T_{\rm lab}$=200 MeV.

forms of the relativistic NN amplitude on the spin observables at various incident energies. Furthermore, this model can be used to generate the scalar and vector optical potentials by folding the components of NN t matrix with the scalar and baryon densities as discussed in Sec. II B.

Essentially this model is a parametrization of the NN t matrix as a sum of Yukawa terms such that both direct and exchange contributions are considered separately. The real and imaginary amplitudes of the direct part of the full t matrix in Table I, expressed as a function of the momentum transfer and effective laboratory kinetic energy $\mathrm{T}_L^{\rm eff}$, are parametrized in the form

$$T_i(\mathbf{q}, T_L^{\rm eff}) = \frac{g_i^2(T_L^{\rm eff})}{m_i^2 + q^2} \left(\frac{\Lambda_i^2(T_L^{\rm eff})}{\Lambda_i^2(s) + q^2} \right)^2 . \tag{7}$$

The exchange contributions to the NN t matrix are similar in form to Eq. (7) with the exception that $\mathbf{q}$ is replaced by the exchange momentum transfer $\mathbf{Q}$. The real and imaginary meson coupling constants g_i^2 and the meson-nucleon cutoff parameters Λ_i^2 are fixed by fitting to the relativistic representation of the NN Arndt phase shifts at each value of $\mathrm{T}_L^{\rm eff}$.

In the past, concern has been expressed about ambiguities in the form of the relativistic NN amplitude [7, 1]. The form shown in Table I is sufficient to parametrize the free NN amplitudes. However, there is no direct experimental information to determine how $\mathcal{M}$ in Eq. (3) will change as the Dirac spinors change from U to U^*. One can make other choices for $\mathcal{T}$ of Eq. (4) which will have the same free spinor matrix elements but different medium modified matrix elements and hence different quasielastic spin observables. One of the major ambiguities concerns the choice of the πN vertex in the amplitudes [7, 17]. One could use either a pseudoscalar vertex which simply uses the five amplitudes in Table I, or a pseudovector vertex. Elastic proton-nucleus spin observables at energies higher than 400 MeV show no difference between pseudoscalar and pseudovector couplings of the pion [18]. At lower energies, however, the differences become larger and the pseudovector coupling is more compatible with the strength and energy dependence of the real scalar and vector optical potentials. Crude calculations [7] of quasielastic $(\vec{p}, \vec{n})$ spin observables at 500 MeV, as well as various theoretical arguments [13] support the pseudovector form . At this stage, however, no overwhelming experimental evidence seems to clearly resolve this ambiguity and hence it is one of the aims of this paper to use the HLF model to investigate this through quasielastic proton-nucleus scattering.

Previously [7] the transition from a pseudoscalar to a pseudovector πN coupling was made by making the following substitutions (referred to as *method A*) in Table I:

$$\lambda_{ps} = \gamma_5 \rightarrow \lambda_{pv} = \frac{q_\mu \gamma^\mu \gamma_5}{2m} , \tag{8}$$

where q^μ is the four-momentum transfer. For free Dirac spinors this implies that matrix elements implicitly contained in Eq. (3) yield

$$(\overline{U}_1\lambda^1_{pv}U_1)(\overline{U}_2\lambda^2_{pv}U_2) = (\overline{U}_1\lambda^1_{ps}U_1)(\overline{U}_2\lambda^2_{ps}U_2)\ , \quad (9)$$

thus giving the same free NN data. In a nuclear medium, the corresponding equality is

$$(\overline{U}^*_1\lambda^1_{pv}U^*_1)(\overline{U}^*_2\lambda^2_{pv}U^*_2)$$

$$= M^*_1M^*_2(\overline{U}^*_1\lambda^1_{ps}U^*_1)(\overline{U}^*_2\lambda^2_{ps}U^*_2)\ , \quad (10)$$

such that the pseudoscalar and pseudovector forms differ by a factor $M^*_1M^*_2$ (recall that $M^* = m^*/m$). This procedure does not explicitly incorporate the meson mediators of the NN force, such as the long range pions, for example, and hence method A is a fairly crude way of treating the different "pion" couplings. In this case, however, the relativistic NN amplitudes are calculated via a relation to a Wolfenstein-type parametrization of the Arndt phase shifts.

A more appropriate way would be to use the HLF model where the direct invariants in Eqs. (7) can be expressed as linear combinations of the five exchange invariants via the Fierz matrix, such that the exchange terms from "pion" can contribute to each type of invariant. For the HLF model the transition from a pseudoscalar to a pseudovector πN vertex is made by performing the following substitution (referred to as *method B*) in all direct and exchange terms in Eq. (4) containing the "pion":

$$g^2_\pi \rightarrow g^2_\pi M^*_1M^*_2\ . \quad (11)$$

In Sec. III the sensitivity of the spin observables is investigated and compared with respect to the use of methods A and B for implementing the pseudoscalar and pseudovector forms of the πN coupling.

The HLF also allows one to consider corrections to the RPWIA due to explicit treatments of exchange. It has been reported [2] that calculations of elastic scattering spin observables at laboratory energies of 500 MeV and higher seem to indicate that exchange contributions are not significant. However, Ref. [18] claims that a proper treatment of exchange is crucial for predicting elastic scattering spin observables at large angles and/or low energies. Hence the effect of exchange needs to be studied for quasielastic proton-nucleus scattering, and hence is investigated in Sec. III for laboratory energies in the 135 to 500 MeV range. Due to the complexity of expressions for the spin observables, it is not obvious as to how they are affected by the inclusion of exchange affects. However, at least one can comment on the behavior of individual exchange terms in Eq. (7). The direct and exchange four-momentum transfers, q and Q, are related by [11]

$$q^2 + Q^2 = T^{\rm eff}_L m/2\ , \quad (12)$$

which means that, for q fixed, as $T^{\rm eff}_L$ is lowered, Q^2 decreases resulting in an increase in the individual exchange terms in Eq. (7) (with q replaced by Q). Similarly, as $T^{\rm eff}_L$ increases, Q^2 increases such that the individual exchange terms become negligible relative to the corresponding direct terms. The manifestation of these effects in the spin observables will be considered in Sec. III.

As published HLF parameters exist unfortunately only at the few $T_{\rm lab}$ values of 135, 200, 300, and 400 MeV [11], we employed for the present calculations the HLF parameter set associated with the values of $T^{\rm eff}_L$ closest to the present incident laboratory energy values. For comparative reasons, the same procedure has been followed for calculations based on method A.

Section III presents calculations based on methods A and B for pseudoscalar and pseudovector forms of the πN vertex.

III. RESULTS

In this section results are presented for quasielastic spin observables using the RPWIA of Sec. II. Calculations are performed for inclusive $(\vec{p},\vec{p}')$ scattering from nuclei in the range ^{12}C to ^{54}Fe and at incident laboratory energies ranging from 135 to 420 MeV. At each energy, the scattering angle was chosen to correspond to a laboratory momentum transfer of 1.97 fm^{-1} in the free NN frame, such that the quasielastic peak is centered at $\omega \approx$ 80 MeV for all incident energies (these angles range from 20° to 50°). The momentum transfer and incident energies were chosen so as to correspond to complete sets of quasielastic spin observable data on ^{16}O and ^{12}C at 420 MeV and ^{12}C at 290 MeV [18] and also due to the availability of HLF parameters at approximately these incident energies.

The first four subsections are devoted to sensitivity studies of the spin observables with respect to different effective masses, different forms of the relativistic NN amplitudes, relativistic effects, and exchange effects. The results of the spin observables will be presented in graphical form to highlight the specific tendency in each of the subsections. Each figure will be a set of six graphs for the six independent spin observables $D_{i'j}$, respectively, all on the same scale. Note that in Figs. 1 to 5 the plot characters refer to our calculated values and the solid and dashed lines serve only to guide the eye along a particular calculated data set. Although these graphs speak for themselves, a few comments will be made in each subsection.

A. Sensitivity to different effective masses

According to Table II, the largest differences between the new effective masses ($M^*_{\rm SC}$ and $M^*_{\rm CP}$) and the original effective masses ($M^*_{\rm HM}$) appear for ^{54}Fe at 290 MeV [19]. Consequently, the sensitivity of the spin observables was investigated for this extreme case, for which $|\mathbf{q}|$ =1.36 fm^{-1} (scattering angle $\approx$ 20°). The results, in terms of the spin observables calculated for the centroid of the quasielastic peak, are shown in Table III. Although not displayed, the similar values for $M^*_{\rm SC}$ and $M^*_{\rm CP}$ in Table II yield practically identical spin observables. The spin observables based on $M^*_{\rm SC}$ show differences of up to 30% compared to calculations using $M^*_{\rm HM}$, the most sensitive observables being $D_{s's}$ and A_y and the least sensitive $D_{l's}$. These large variations illustrate the importance of using more refined calculations of the effective masses. Consequently, from now on all calculations will use the

TABLE III. Values of the spin observables at the centroid of the quasielastic peak ($\omega = \mathbf{q}^2/2M$), for inclusive ^{54}Fe($\vec{p},\vec{p}'$) $T_{\rm lab}$=290 MeV at momentum transfer of 1.36 fm^{-1}, for different values of the effective masses in Table I.

Effective masses	A_y	$D_{n'n}$	$D_{s's}$	$D_{l'l}$	$D_{s'l}$	$D_{l's}$
M	0.418	0.602	0.105	0.140	0.207	0.194
$M^*_{\rm HM}$	0.317	0.582	0.366	0.232	0.347	0.394
$M^*_{\rm SC}$	0.278	0.550	0.459	0.249	0.319	0.392
$M^*_{\rm CP}$	0.280	0.546	0.454	0.244	0.310	0.383

new, more refined, $M^*_{\rm SC}$ values (now denoted by only M^*) in Table II.

B. Sensitivity to different forms of the NN amplitudes

In this subsection we use and compare both methods A and B, discussed in Sec. II D, to investigate the sensitivity of the spin observables at the centroid of the quasielastic peak to both pseudoscalar and pseudovector choices of the "pion". Here and in Secs. III C and III D, we employ ^{40}Ca as the scatterer nucleus, being the nucleus formerly best studied, for investigating overall trends in spin observables. We introduce $D^{\rm PS}_{i'j}(M^*)$ and $D^{\rm PV}_{i'j}(M^*)$ to refer to spin observables calculated by using respectively a pseudoscalar (PS) or a pseudovector (PV) coupling for the "pion", both calculated with an effective mass M^*. It is obvious from Eq. (10) for method A and Eq. (11) for method B that calculations based on PS(M) and PV(M) treatments of the pion yield identical spin observables. Hence only $D^{\rm PS}_{i'j}(M)$-based results will be quoted when necessary.

We now proceed to show the importance of using the HLF model (method B), as opposed to method A, when investigating the sensitivity of the observables to different forms of the pseudoscalar amplitude, especially at low energies. Figure 3 compares for all spin observables $D_{i'j}$ the values of $|D^{\rm PV}_{i'j}(M^*) - D^{\rm PS}_{i'j}(M^*)|$ calculated by method A (dashed lines) and method B (solid lines). Values of the statistical experimental errors are typically about $\pm$ 0.03 [18], therefore a spin observable can be classified as being sensitive to the form of the πN vertex only if $|D^{\rm PV}_{i'j}(M^*) - D^{\rm PS}_{i'j}(M^*)|$ is significantly larger than 0.06.

At energies lower than 200 MeV, $D_{n'n}$ is the most sensitive observable to the $|D^{\rm PV}_{i'j}(M^*) - D^{\rm PS}_{i'j}(M^*)|$ values, as calculated by method B. However, for method A this observable shows minimum sensitivity to this value. A similar tendency, although to a smaller extent, is exhibited by $D_{l's}$. This illustrates the importance of using the more appropriate HLF model (method B), instead of the crude method A. However, at these low energies the remaining spin observables show hardly any sensitivity to the PS versus PV ambiguity for both methods A and B, which justifies the use of only the more crude method A for these spin observables.

At energies higher than 200 MeV, the spin observables $D_{n'n}$ and $D_{l'l}$ are sensitive to the values of $|D^{\rm PV}_{i'j}(M^*) - D^{\rm PS}_{i'j}(M^*)|$, as predicted by both methods A and B, although the sensitivity of $D_{n'n}$ becomes less enhanced. All the other observables are, however, insensitive to this PS(M^*) versus PV(M^*) ambiguity.

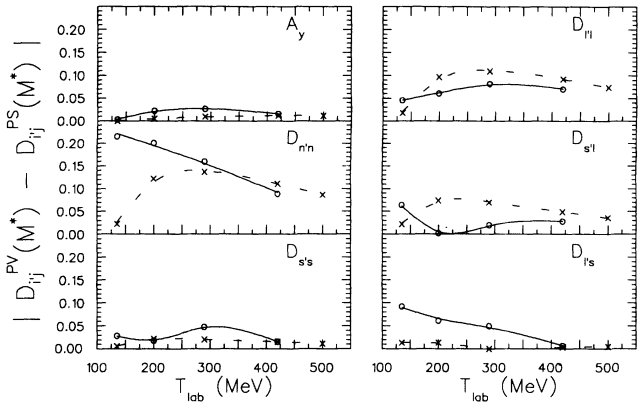

FIG. 3. The difference, $|D^{\rm PV}_{i'j}(M^*) - D^{\rm PS}_{i'j}(M^*)|$, between the spin transfer observables $D_{i'j}$ calculated with a pseudovector (PV) and a pseudoscalar (PS) term in the NN interaction, respectively, as a function of laboratory energy and at the quasielastic peak. The crosses represent calculations based on method A (relativistic parametrization of Arndt phases) whereas the open circles are calculated using method B (HLF model). The solid and dashed lines serve merely to guide the eye.

C. Sensitivity to relativistic effects

In this investigation, we keep the form of the πN vertex fixed, say PS(M^*), and study the difference between effective mass and free mass calculations. Figure 4 displays the energy variation of $|D^{\rm PS}_{i'j}(M^*) - D^{\rm PS}_{i'j}(M)|$ values which serves at present as a measure of the sensitivity to relativity of the specific spin observable $D_{i'j}$. These $|D^{\rm PS}_{i'j}(M^*) - D^{\rm PS}_{i'j}(M)|$ values have been calculated using only method B. (In principle method A should yield identical results for pseudoscalar calculations.) At all energies, the observable $D_{s's}$ exhibits clearly the highest sensitivity to relativity and this effect even increases

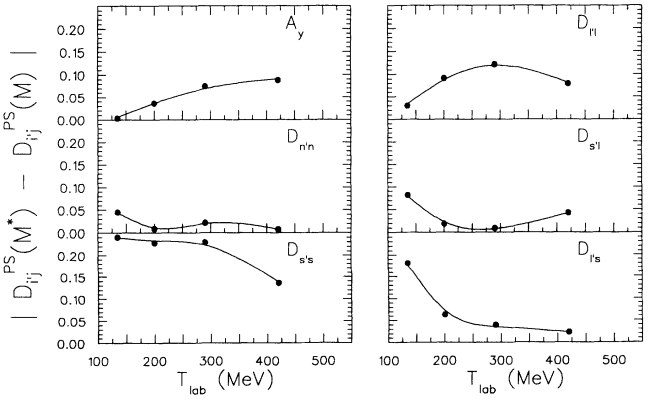

FIG. 4. The same as for Fig. 3, except that here the value of $|D^{\rm PS}_{i'j}(M^*) - D^{\rm PS}_{i'j}(M)|$ is plotted, using only method B.

towards the lower energies. At low energies $D_{l's}$ also shows a considerable relativistic sensitivity but, surprisingly, the analyzing power shows hardly any effect, despite its significant relativistic effects at high energies. All the other spin observables are fairly insensitive to relativistic effects.

D. The effects of exchange

As already mentioned in Sec. II D, at lower energies exchange contributions could become important to the NN amplitudes. To illustrate the effect of exchange at various incident energies, calculations using the full direct plus exchange amplitudes of the HLF model are compared to those where the exchange contribution is completely ignored. Figure 5 illustrates the absolute differences between the latter calculations. Note that for this exercise we chose the PS(M^*) form of the πN vertex; a PV(M^*) choice leads to similar differences. We see that at lower energies the exchange contributions to the amplitudes generally become important; in particular, $D_{s'l}$ and $D_{l'l}$ start showing extreme sensitivity to exchange effects. This illustrates the importance of using the HLF model at low energies, as opposed to the Wolfenstein-type parametrizations which cannot separate the NN amplitudes into direct and exchange parts.

E. Predictions to data

After studying the behavior of the quasielastic spin observables to the above-mentioned effects at the quasielastic peak, we are in a position to compare calculations to data and to realize the limitations of the methods used. Results are compared to data on ^{12}C at $T_{\rm lab}$ = 290 and 420 MeV at angles which correspond to a lab momentum transfer of 1.97 fm^{-1} in the free NN system, in order to center the quasielastic peak at $\omega \approx 80$ MeV for both laboratory energies [19]. The results (using $M_{\rm SC}^{\rm eff}$ effective mass values) are displayed in Figs. 6 and 7 for $T_{\rm lab}$ = 420 and 290 MeV respectively, and include spin-orbit distortions. The solid lines represent the free mass calculation whereas the dotted and dashed lines represent respectively the relativistic PS(M^*) and PV(M^*) results using effective masses from Table II. Note from Fig. 3 that, at these high energies, relativistic results of the HLF model (method B) and those related to Wolfenstein-type parametrizations (method A) are very similar. For this reason and also due to the lack of HLF parameter sets at most effective laboratory kinetic energies, the use of the HLF model is not justified; instead we perform calculations in a manner similar to Ref. [2], i.e., using method A and calculating the amplitudes at every value of the effective laboratory kinetic energy. At 420 MeV (Fig. 6), $D_{n'n}$ is the most sensitive observable to the PS(M^*) versus PV(M^*) ambiguity. Although the PS(M^*)-based calculation seems to be closer to the data, the free mass prediction definitely favors the data. Within the statistical error bars, all the other observables are insensitive to the form of the πN coupling. None of the predictions agree with the $D_{s's}$ data. $D_{l'l}$ is slightly more favorable towards relativity. However, $D_{s'l}$ and $D_{l's}$ are insensitive to any differences between effective mass and free mass predictions. In general one can conclude that, except for A_y, both relativistic and free mass calculations

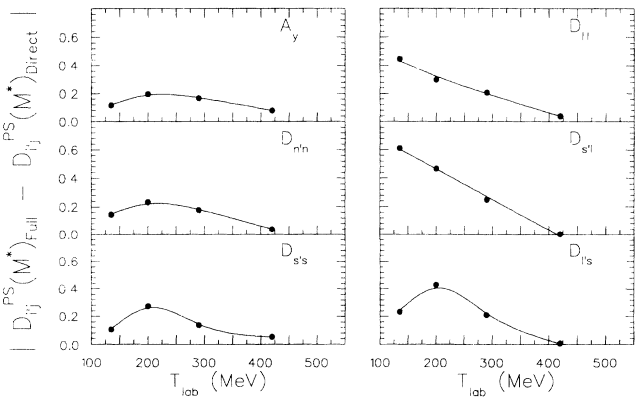

FIG. 5. Same as for Fig. 4, except that here the value of $|D_{i'j}^{\rm PS}(M^*)_{\rm Full} - D_{i'j}^{\rm PS}(M^*)_{\rm Direct}|$ is plotted as a closed circle. The subscript "Direct" refers to calculations where the exchange terms have been neglected, whereas the subscript "Full" indicates inclusion of exchange.

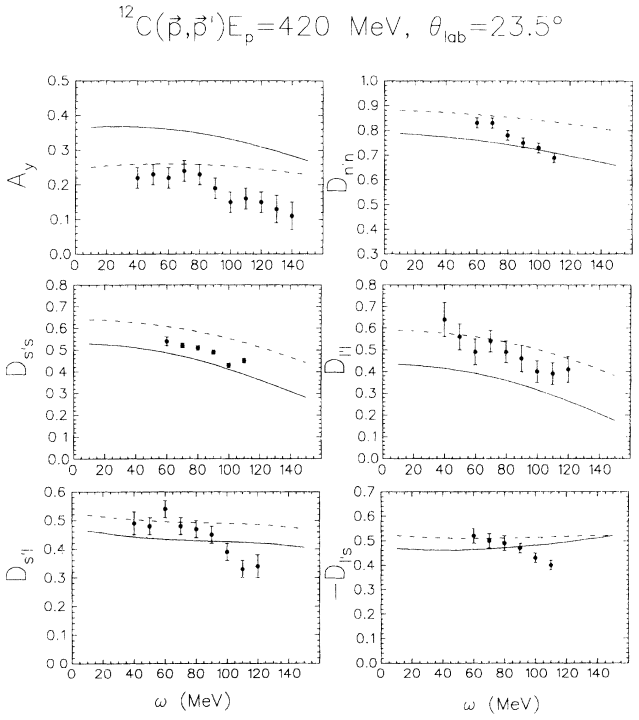

FIG. 6. Spin observables for a range of transferred energy ω over the quasielastic peak for inclusive proton scattering from ^{12}C at 420 MeV and $\theta_{\rm lab}$=23.5°. The centroid of the quasielastic peak is at $\omega \approx 80$ MeV. Data are from Ref. [18], where P and A_y refer to induced polarization and analyzing power, respectively. The solid line represents the free mass calculation whereas the dotted and dashed lines represent, respectively, the relativistic PS(M^*) and PV(M^*) results using effective masses from Table II.

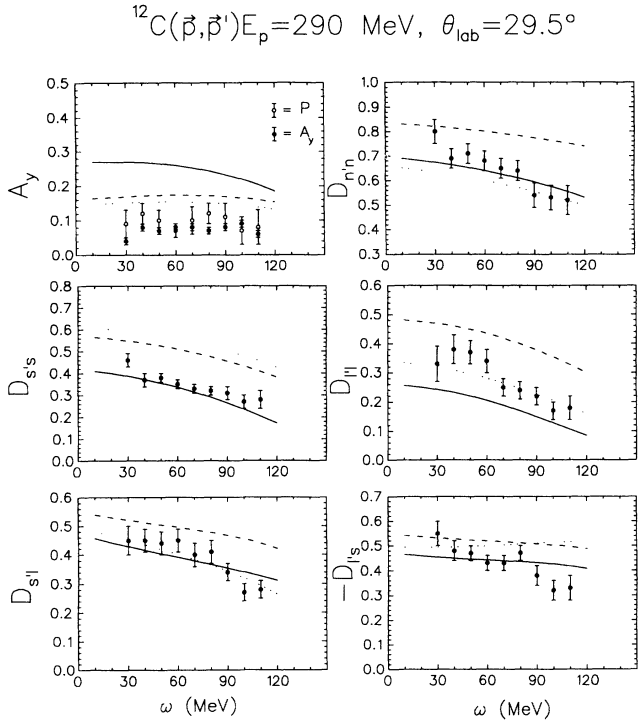

FIG. 7. The same as for Fig. 6, except for 290 MeV proton scattering at θ_{lab}=29.5°.

do equally well in predicting the data. Both calculations fail to reproduce $D_{s's}$.

At 290 MeV (Fig. 7) similar trends exist for A_y and $D_{n'n}$. However, $D_{s's}$ displays a clear free mass effect signature, whereas $D_{l'l}$ definitely favors a PS(M^*)-based relativistic calculation. For $D_{s'l}$ both the PS(M)- and the PS(M^*)-based relativistic calculations do equally well in reproducing the data. $D_{l's}$ seems to be slightly more favorable to a free mass prediction. We also see that most spin observables correctly predicted at the centroid of the quasielastic peak for 290 and 420 MeV are fairly well reproduced over most of the ω range of the broad peak, thus emphasizing the validity of the simple Fermi gas model approach of the nucleus at these momenta transfer. Whereas at 420 MeV many of the observables show no preference to the major effects we presently investigate, some of these observables become slightly more enhanced to these effects at lower energies. However, this enhancement is not very drastic and even at 290 MeV there are still a few observables that remain insensitive to certain effects. Recall from the preceding sections that the most suitable laboratory energies to exploit the sensitivity of the spin observables are 200 MeV and below. For this reason data at these low energies are crucial in investigating questions such as relativistic M^* effects and the different forms of the πN vertex.

IV. CONCLUSIONS

We finally comment on the sensitivity of the spin observables to the combination of the above-mentioned effects. In doing so, spin observables are identified which show enhanced sensitivity to only one of the effects; the other effects being negligible.

In general we have seen that one must use a model, such as the HLF model (method B) for the relativistic NN amplitudes, in order to calculate spin observables meaningfully at low energies. At high energies methods A and B yield similar results. Looking globally at the presently considered forms of the πN vertex in the NN interaction, the allowance of relativity in the formalism, the inclusion of exchange, and the effects of spin-orbit distortions, the following general trends become clear:

At low energies $D_{n'n}$ is by far the most sensitive to the relativistic PV versus PS form of the pion coupling. Spin-orbit distortions have no effect on this observable, and effective mass versus free mass predictions (with the πN vertex fixed) are practically the same.

Also at low energies $D_{s's}$ shows enhanced sensitivity to relativity, whereas it cannot significantly distinguish between different forms of the pseudoscalar amplitude, and the effect of spin-orbit distortion is small.

The above-mentioned trends do persist at higher energies, but are less enhanced against the statistical errors. At high energies, however, A_y is very sensitive to relativistic effects, a fact previously established, whereas at low energies this observable is insensitive to relativity and to different forms of the πN vertex.

The sensitivity of the spin observables $D_{s'l}$ and $D_{l'l}$ to exchange at low energies completely overshadows any of the above-mentioned effects and thus indicate the importance of including exchange.

No observable shows enhanced sensitivity with respect to spin-orbit distortions compared to the above-mentioned effects. Typically the effects of spin-orbit distortions are of the same size if not smaller than the statistical errors.

Thus, at energies lower than and equal to 200 MeV, we have established the importance of the quasielastic spin observables $D_{n'n}$, $D_{s's}$, $D_{s'l}$, and $D_{l'l}$ in studying relativity, the medium modified NN interaction, the form of the πN vertex, and the importance of exchange. Therefore, we stress the urgent need for measurements of any of these observables at low energies in providing guidance to the understanding of these effects.

Now that we have established the sensitivity of the quasielastic spin observables to the various effects, one needs to calculate them quantitatively at low energies. In order to accomplish this, one requires HLF parameter sets at small intervals of incident beam energies. At present these parameter sets are being generated by fitting to free NN scattering data.

Recently [20] it has been reported, for quasielastic $(\vec{p},\vec{n})$ scattering at 290 and 420 MeV, that A_y is better described nonrelativistically. It would be interesting to perform more refined relativistic calculations of the spin observables for quasielastic $(\vec{p},\vec{n})$ charge-exchange reactions at large momentum transfers. Such reactions are complementary to quasielastic $(\vec{p},\vec{p}')$ reactions in that they sample only the isovector part of the NN interaction.

ACKNOWLEDGMENTS

The authors would like to thank the theory group at the University of Indiana, especially C. Horowitz, for the very kind hospitality. Special financial support to G.C.H. by the South African FRD and Harry Crossley Foundation, and to P.R.deK. by the University of Stellenbosch, is gratefully acknowledged.

[1] C. J. Horowitz, in *Proceedings of the International Conference on Spin and Isospin in Nuclear Reactions, Telluride, Colorado, 1991*, edited by S. W. Wissink, C. D. Goodman, and G. E. Walker (Plenum, New York, 1991), p. 415.

[2] J. A. McNeil, J. R. Shepard, and S. J. Wallace, Phys. Rev. C **50**, 1439 (1983).

[3] O. V. Maxwell and E. D. Cooper, Nucl. Phys. **A513**, 584 (1990).

[4] R. de Swiniarski, D. L. Pham, and J. Raynal, Z. Phys. A **343**, 179 (1986).

[5] E. D. Cooper, S. Hama, B. C. Clark, and R. L. Mercer, Phys. Rev. C **47**, 297 (1993).

[6] C. Alvarez, H. F. Arellano, F. A. Brieva, and W. G. Love, in *Proceedings of the International Conference on Spin and Isospin in Nuclear Reactions, Telluride, Colorado, 1991*, edited by S. W. Wissink, C. D. Goodman, and G. E. Walker (Plenum, New York, 1991), p. 219.

[7] C. J. Horowitz and D. P. Murdock, Phys. Rev. C **37**, 2032 (1988).

[8] H. Esbensen and G. F. Bertsch, Phys. Rev. C **34**, 1419 (1986).

[9] C. Chan, T. E. Drake, R. Abegg, D. Frekers, O. Häusser, K. Hicks, D. A. Hutcheon, L. Lee, C. A. Miller, R. Schubank, E. J. Stephenson, and S. Yen, J. Phys. G **15**, L55 (1989).

[10] C. J. Horowitz and M. J. Iqbal, Phys. Rev. C **33**, 2059 (1986).

[11] C. J. Horowitz, Phys. Rev. C **31**, 1340 (1985).

[12] J. D. Bjorken and S. Drell, *Relativistic quantum mechanics* (McGraw-Hill, New York, 1964).

[13] B. D. Serot and J. D. Walecka, in *Advances in Nuclear Physics*, edited by J. W. Negele and E. Vogt (Plenum, New York, 1986), Vol. 16, p. 116.

[14] M. J. Iqbal, in *Proceedings of the International Conference on Spin Observables of Nuclear Probes, Telluride, Colorado, 1988*, edited by C. J. Horowitz, C. D. Goodman, and G. E. Walker (Plenum, New York, 1991), p. 53.

[15] A. M. Kobos, E. D. Cooper, J. I. Johansson, and H. S. Sherif, Nucl. Phys. **A445**, 605 (1985).

[16] C. J. Horowitz, D. P. Murdock, and B. D. Serot, in *Computational Nuclear Physics I*, edited by K. Langanke, J. A. Maruhn, and S. E. Koonin (Springer-Verlag, Berlin, 1991), p. 129.

[17] D. P. Murdock and C. J. Horowitz, Phys. Rev. C **35**, 1442 (1987).

[18] C. Chan, T. E. Drake, R. Abegg, D. Frekers, O. Häusser, K. Hicks, D. A. Hutcheon, L. Lee, C. A. Miller, R. Schubank, and S. Yen, Nucl. Phys. **A510**, 713 (1990).

[19] O. Häusser, R. Abegg, R. G. Jeppesen, R. Sawafta, A. Celler, A. Green, R. L. Helmer, R. Henderson, K. Hicks, K. P. Jackson, J. Mildenberger, C. A. Miller, M. C. Vetterli, S. Yen, M. J. Iqbal, and R. D. Smith, Phys. Rev. Lett. **61**, 822 (1988).

[20] K. H. Hicks, W. P. Alford, A. Celler, R. S. Henderson, K. P. Jackson, C. A. Miller, M. C. Vetterli, S. Yen, F. Brieva, C. J. Horowitz, and J. Piekarewicz, Phys. Rev. C **47**, 260 (1993).